Vibrational Energy Relaxation of the OH Stretch in Liquid Methanol

Tolga S. Gulmen and Edwin L. Sibert, III*

Department of Chemistry and Theoretical Chemistry Institute, University of Wisconsin - Madison, Madison, Wisconsin 53706

Received: November 10, 2003; In Final Form: January 6, 2004

The state-to-state rate of vibrational energy relaxation of the OH-stretch fundamental is investigated via perturbative methods. The system is separated into an 11 degree of freedom methanol molecule and the surrounding bath. Notably, the large amplitude torsional motion is considered a bath degree of freedom, and the 11 small amplitude normal modes are expanded in a Fourier series of the torsional angle. The methanol-bath coupling is computed through the use of a molecular dynamics simulation, and the results are computed using Landau−Teller and time dependent perturbation theory. Results are compared to the ultrafast pump−probe experiments of L. K. Iwaki and D. D. Dlott [*J. Phys. Chem. A* **2000**, *104*, 9101].

I. Introduction

Vibrational energy relaxation (VER) in liquids is a central component of reaction dynamics.[1−3] The ability of molecules to redistribute energy into internal degrees of freedom following reactions or laser excitation is a key component in product stabilization. Understanding this relaxation from a molecular perspective will shed new light on the fluctuating forces a solute molecule experiences in its liquid environment.

In the past few years, experiments have yielded a wealth of information on VER.[4] Studies have ranged from deuterated water[5−8] and the azide ion[9] to watching energy flow spatially along molecular backbones.[10] The role of the density of states and intramolecular couplings have been highlighted by examining VER trends for the iodomethane[11] and haloform series[12−16] as well as by comparing VER following fundamental and overtone excitation.[17] The influence of solvent−solute couplings has been probed by varying solute polarity for iodomethanes[17] and by varying solute concentrations of hydrogen bonding species that span monomeric or small clusters in apolar solvents[18−22] all the way to neat hydrogen bonding liquids such as methanol.[23] Detailed comparisons of gas- and liquid-phase VER[24,25] have underlined the sometimes important contribution of intramolecular vibrational relaxation in the gas phase to VER in liquids. While this is not a comprehensive list, it does indicate the variety of problems being investigated.

On the theoretical side, VER has been studied using centroid dynamics[26,27] and instantaneous normal modes.[28] The former allows one to include quantum effects in the solvent−time correlation functions, and the latter allows insights into solute−solvent interactions. By far the most prevalent method, however, for treating realistic systems has been Landau−Teller theory (LT). This is due to its simplicity and success at explaining a variety of VER phenomena in polyatomic molecules.[2,29−34] In this theory, which is based on linear response theory, population is transferred between the quantum mechanical energy levels of a solute molecule due to the time-dependent perturbations between the solute and the classical solvent. The challenge in applying this theory is that one needs accurate descriptions of the intermolecular solute−solvent couplings and intramolecular solute couplings. Given these couplings, one must then calculate the vibrational energy levels of the solute and compute the many solvent correlation functions. As the molecular systems of interest increase in size and chemical complexity, these tasks become increasingly challenging.

In this paper, we apply Landau−Teller theory to the study of vibrational relaxation following excitation of the OH stretch in neat methanol. There are several reasons for this choice. Neat methanol and HOD in D_2O share several features, and hence we can expect to build on the results of previous research.[31,34] Methanol and water both have broad OH stretch fundamental bands due to hydrogen bonding. They also have OH bending vibrations of approximately the same energy. The relaxation of the OH stretch of HOD in D_2O has been theoretically predicted[31,34] to proceed via excitation of the overtone of the bend, a transition referred to as a $\Delta v = 3$ process as the OH stretch and overtone bend differ by three quanta of excitation. We can anticipate that a similar pathway will apply for methanol. Methanol, however, has a much higher density of states, with the result that many states lie within the broad band feature of the OH fundamental. Thus, MeOH relaxation might be more similar to that found for $CHCl_3$, where there is a flow of energy to a nearly degenerate state that involves a $\Delta v = 4$ process.[33] One can anticipate that the situation is even more complicated since the large solvent-induced energy level fluctuations will lead to avoided crossings between the OH fundamental and background states. Under these circumstances it is unclear whether the average energy difference used in LT theory will lead to accurate rates. For this reason we also solve the time-dependent Schrödinger equation (TD) as an alternative approach to calculating rates.

While water is the liquid of life, MeOH is often easier to investigate because of the fewer number of hydrogen bonds per molecule and the fact that the methyl group in MeOH allows it to be dissolved in a wider variety of apolar solvents. This has led to a variety of experimental studies. Dilute MeOH in CCl_4 experiments[35,36] shows that VER is intimately related to hydrogen bond dynamics. Not only is ν(OH) vibrational excitation able to disrupt hydrogen bond networks, but also the relaxation time scale for monomeric MeOH is a factor of nine[36] and monomeric MeOD is a factor of two[18] slower than that of the

* Corresponding author. E-mail: sibert@chem.wisc.edu.

10.1021/jp037417m CCC: $27.50
Published on Web 03/10/2004

neat liquid MeOH which appears to be about one picosecond.[23] Even in the neat liquid, Iwaki and Dlott have shown that by tuning the IR-pump laser they can excite subsets of molecules with different environments as revealed by the remarkably different VER associated with the IR-pump frequency.[23]

We find that the relaxation time constants are 2.7 and 3.1 ps for LT and TD, respectively. Inclusion of a quantum correction factor in the LT result reduces the lifetime to 1.6 ps. Despite the similarity of results, there are notable differences at the level of state-to-state relaxation dynamics. These differences are due to the solvent-induced energy level fluctuations of the solute molecule. Our results are slower than the experimentally observed 0−1 ps time constant,[23] but strongly interacting solutes have consistently been slower in calculations.[31,34] We find that relaxation of the OH fundamental occurs mainly through the OH bend overtone; however, near degenerate combination states contribute significantly to the relaxation with the result that all modes are excited in the initial onset of relaxation as is found experimentally.[23] In the TD approach, laser excitation is included to prepare the initial state so that one can avoid any approximations made with regard to initial state excitation. We are also able to selectively excite subsets of states by tuning the frequency of the excitation laser. We find an enhancement of the bend population for the red-shifted laser excitation that is consistent with that found experimentally.[23]

A shortcoming of the present work is that it will not correctly treat vibrational relaxation that leads directly to breaking of the hydrogen bond. This relaxation mechanism for the OH stretch in HOD/D_2O has been theoretically investigated using simple models that treat the hydrogen bonding mode quantum mechanically.[37] The results suggest[2] that this mechanism may be operative for HOD/D_2O. Experimental results suggest that this pathway for relaxation is not relevant for OH relaxation in neat methanol.[23]

The paper is laid out as follows. We begin by providing background material for the methanol system and describe the methods that are used in this work. These methods include the isolated molecule quantum calculation, the molecular dynamics simulation, and outlines of the Landau−Teller theory and time-dependent theory. Having presented the models we then present and discuss the results.

II. Background

To understand energy flow in MeOH we begin with a review of the nature of the vibrations themselves. The gas- and liquid-phase vibrational frequencies of MeOH are compared in Table 1. The 11 small amplitude vibrations include 5 stretches, 4 bends, and 2 rocking modes. The symbols ν, δ, and ρ distinguish these respective motions. Although the symmetry of the vibrations is defined with respect to C_s symmetry with an *s* or *a* subscript, the numbering is not. The most noticeable change between the gas- and liquid-phase is that the ν(OH) shifts from a sharp peak at 3686 cm^{-1} to a several hundred wavenumber broad peak around 3400 cm^{-1}, this being a typical signature of hydrogen bonding.

Iwaki and Dlott investigated VER pathways[23] and time scales in neat MeOH via an IR pump/Raman probe experiment. The experiment monitors population in all the molecular vibrations, since they are all Raman active. The results in Figure 1 arise from pumping the ν(OH) with a mid-IR pulse and probing the anti-Stokes Raman signal with a 532 nm laser. Both laser pulses have a duration of approximately 0.8 ps. It should be noted that it is nontrivial to obtain the relative populations from the anti-stokes intensity; there is both overlap of the vibrational transitions and simultaneous signal from overtones, combination bands, and fundamentals, each of which has a different frequency due to anharmonicities.

TABLE 1: Comparison of Theoretical and Experimental Vibrational Energies (in cm^{-1}) for Methanol[a]

		gas phase			liquid phase		
state	motion	harmonic	2nd	expt.[b]	2nd	adjusted	expt.[c]
1_1	ν(OH)	3883.8	3686.3	3685.3	3585.4	3400.1	3400
2_1	ν_s(CH)	3014.1	2831.8	2838.6	2833.1	2833.8	2834
3_1	δ_s(CH)	1489.9	1453.0	1453.3	1468.4	1468.3	1466
4_1	δ(OH)	1367.9	1349.2	1320.6	1379.8	1381.7	1381
5_1	ν(CO)	1068.3	1036.0	1028.4	1052.9	1033.9	1034
6_1	ν_a(CH)	3100.6	2994.4	2997.6	3004.5	3004.5	2944
7_1	δ_a(CH)	1513.8	1476.6	1474.8	1487.1	1487.0	1541
8_1	$\rho_a(CH_3)$	1114.5	1082.6	1073.2	1115.6	1115.9	1117
9_1	ν_a(CH)	3092.2	2958.6	2955.1	2975.5	2975.4	
10_1	δ_a(CH)	1514.2	1474.7	1473.9	1486.6	1486.6	
11_1	$\rho_a(CH_3)$	1187.0	1160.9	1150.5	1172.5	1172.4	

[a] Theoretical energies are calculated with second-order perturbation theory. [b] From ref 61, ν_1; ref 62, ν_6, ν_2, and ν_9; ref 63, ν_7; ref 64, ν_3 and ν_{10}; ref 65, ν_4; refs 66 and 67, ν_8, ν_5, and ν_{11}. [c] From ref 23.

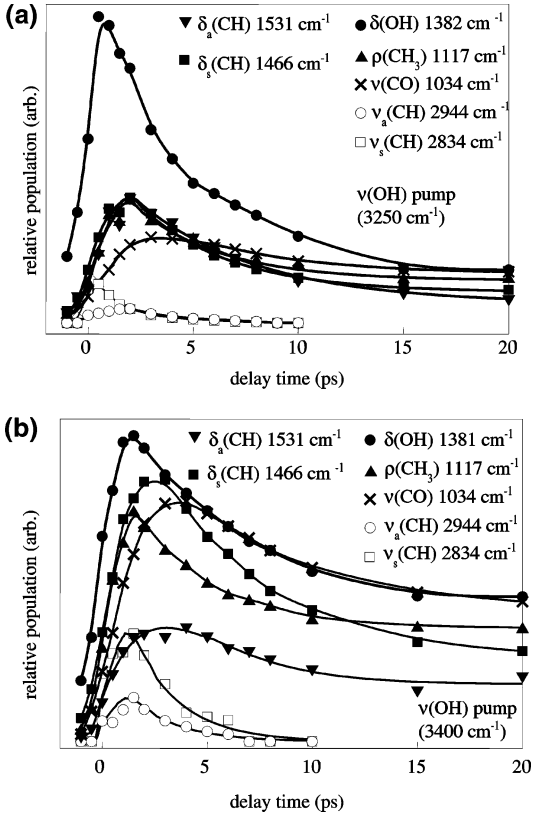

Figure 1. Population in the spectrally distinct normal modes as a function of time following excitation of the OH fundamental. Results are those of Iwaki and Dlott.[23] (a) Corresponds to 3250 cm^{-1} excitation; (b) corresponds to 3400 cm^{-1} excitation. See text for further details.

The results of Figure 1 are for IR-pump frequencies (top) 3250 and (bottom) 3400 cm^{-1}, respectively. The OH relaxation (not shown) occurs within one picosecond for both measurements, this being near the temporal detection limit. There are two key similarities between these two figures. First, all vibrational modes exhibit excitation within 1 ps. This is in contrast to excitation of the ν(CH)'s at 2870 and particularly at 2970 cm^{-1}.[23] In those cases, there was no initial buildup of population in the lower energy $\rho(CH_3)$ and ν(CO) modes, and most of the energy was deposited into δ(OH). Second, the δ-(OH) vibration has the largest relative population, while the ν-(CH)'s have the smallest relative population. The central

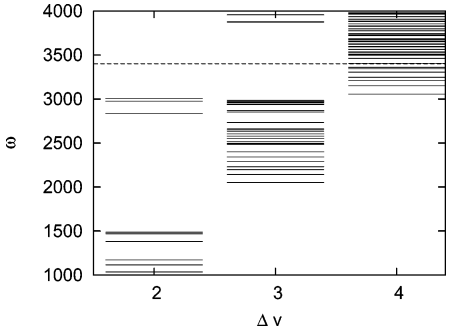

Figure 2. Schematic of vibrational energy levels organized by Δv, the total difference in vibrational quanta between a given state and the OH fundamental.

difference between the two figures is that δ(OH) is more readily excited with the lower frequency pump laser.

The goal of this paper is to elucidate the above findings using a combination of LT and TD theories. Our study focuses on the initial stage of vibrational relaxation, as this is where the perturbation theory treatments are amenable. Moreover, in the early stage of transfer, vibrational energy transfer to other molecules (VET) is an exceedingly small component of the dynamics. Iwaki and Dlott examined this with the same pump/probe setup, but this time using a solution of 75% MeOH and 25% CCl_4 and monitoring three vibrational modes of CCl_4. Regardless of pump frequency or mode monitored, full CCl_4 buildup happened within 20 ps with no initial burst of buildup at time zero. This results suggests that the initial dynamics are almost entirely intramolecular.[23] This is consistent with the theoretical model of Staib[38] who examined near resonant transfer of OH excitation among methanol molecules. The relaxation rate out of the OH stretch was found to be significantly slower than the observed rate. As the model contains only a single degree of freedom per molecule, the OH stretch, Staib concluded that the near resonant transfer to overtones and combination bands must be decisive.

To introduce the ideas of VER out of ν(OH), and to show which particular overtones and combination bands are likely to be important we show Figure 2 in which vibrational energies of liquid MeOH are plotted versus the change in vibrational quantum number from the ν(OH), at 3400 cm^{-1}, to the other vibrational eigenstates of the small amplitude motions between 1000 and 4000 cm^{-1}.

In this window, the $\Delta v = 2$ processes correspond to transitions to the other 10 fundamentals. If the intermolecular couplings to these modes were the same, then one would expect the ν(CH)'s to be the most important states, since these modes have the highest frequency. However, in a ball and spring picture the ν(OH) and the ν(CH)'s are indirectly coupled through the ν(CO), and so one can anticipate small couplings.

Figure 2 shows that there are no near resonant states with $\Delta v = 3$. In fact the $\Delta v = 2$ CH fundamentals are more nearly resonant. There is a window almost 1000 cm^{-1} wide centered around the excitation frequency of the OH stretch. Below 3400 cm^{-1}, the transitions to the overtones and combinations of CH and OH bends have the smallest energy mismatch. Of these states, we anticipate that the overtone in the OH bend is likely to be most important, based on the HOD results of Rey and Hynes[31] and Lawrence and Skinner.[34] The states above 3400 cm^{-1} include combination bands with one quantum of CH stretch and one quantum of a rocking mode or CO stretch. Transitions to these states are unlikely, as they require the bath to supply about $2kT$ of energy.

In contrast to $\Delta v = 3$, there is no gap in the $\Delta v = 4$ states at energies near 3400. As one progresses up this stack of states, one proceeds from states that have three quanta of excitation in the CO stretch and rocking modes to states that have two quanta of excitation in these modes and one quanta of excitation in an OH or CH bend. At the higher energies there are states with one quantum in either the CO stretch and rocking modes and two quanta in the bending modes. Any transition between these states only requires a small amount of energy transfer to or from the low-frequency bath states, thus we anticipate that these states may have an important role in the relaxation pathway.

The experiment[23] suggests that all of the above processes are occurring to some extent, since all the modes light up at short times. They also suggest that the $\Delta v = 2$ is least likely. In the following sections, we calculate the eigenstates, that correspond to the eigenvalues shown in Figure 2, and then calculate the rate of flow into these states by determining the time-dependent solute/solvent coupling between them.

III. Landau−Teller and Time-Dependent Approaches

Landau−Teller theory is a perturbation theory based on linear response.[2,39] It allows one to use equilibrium dynamics to describe a nonequilibrium system based on correlation functions and their spectral Fourier transforms. To obtain the LT rate, one computes the rate constant as the Fourier transform of the interaction autocorrelation function at the frequency difference of the states of interest, thus

$$k_{mn}^{LT} = Q(\omega_{mn})\frac{\hat{C}(\omega_{mn})}{\hbar^2} \tag{1}$$

where

$$\hat{C}(\omega) = \int_{-\infty}^{\infty} dt\, e^{-i\omega t}\langle V_{mn}(t)\, V_{mn}(0)\rangle \tag{2}$$

Here $V_{mn} = \langle m|V|n\rangle$ is the bath-dependent coupling obtained by integrating the solute/bath coupling over the solute degrees of freedom where $|m\rangle$ and $|n\rangle$ are the initial and final solute eigenstates, respectively. The average energy difference between these states is ω_{mn}, and $Q(\omega_{mn})$ is the quantum correction factor (QCF) evaluated at ω_{mn}.

Implementation of the theory requires that we partition the Hamiltonian into its various components, find the quantum eigenstates $|n\rangle$ of the vibrational Hamiltonian, and carry out the MD simulation for the bath.

A. Partitioning the Hamiltonian. As in previous vibrational relaxation studies that have used Landau−Teller theory, the system is comprised of a solute molecule interacting with a bath of solvent molecules. As such, the Hamiltonian must be expressed as a sum of three contributions

$$H = H_s + H_b + V \tag{3}$$

describing the solute MeOH vibrational Hamiltonian, the bath Hamiltonian, and the interactions between them, respectively. In this section we describe how we implement this division. We will consider the kinetic and potential contributions in order.

To express the kinetic contribution to the Hamiltonian in the form of eq 3, we begin with a kinetic energy operator describing N MeOH molecules

$$T = \sum_{i=1}^{N} T_i^{mol} \tag{4}$$

Here T_i^{mol} is the kinetic energy contribution in Cartesian coordinates for each molecule. These operators can be written in the form

$$T_i^{\mathrm{mol}} = T_i^{\mathrm{vib}} + T_i^{\mathrm{rot-tor}} + T_i^{\mathrm{tr}} \tag{5}$$

following relatively standard treatments in which the atomic positions are reexpressed as functions of the normal, torsional, rotational, and translational coordinates. With the exception of certain Coriolis and centrifugal coupling terms, this separation is exact. We further assume that intermolecular vibrational−vibrational energy transfer is not important. With this approximation, we can choose to focus on the *j*th molecule by neglecting the vibrational kinetic energy of the remaining $N-1$ MeOH molecules by setting the vibrational kinetic energy equal to zero.

To write the kinetic energy in the form of eq 5, we take as our starting point the kinetic energy contribution to MeOH rotation−vibration−torsion Hamiltonian.[40−42] For the *i*th molecule, it takes the form

$$T_i^{\mathrm{mol}} = \frac{1}{2}(\mathbf{J}^T - \pi)\mu(\mathbf{J} - \pi) + \frac{1}{2}\mathbf{P}^T\mathbf{P} + T_i^{\mathrm{tr}} \tag{6}$$

Here angular momentum operators $\mathbf{J}$ and π have a fourth element, the momentum conjugate to τ. The i subscript is omitted on the momentum terms to simplify notation. We neglect both the Coriolis and centrifugal terms by setting $\mathbf{J}^T\mu\pi = 0$ and $\mu = \mu_e$, respectively. With these approximations, eq 6 becomes

$$T_i^{\mathrm{mol}} = \frac{1}{2}\mathbf{P}^T\mathbf{P} + \frac{1}{2}\pi^T\mu_e\pi + \frac{1}{2}\mathbf{J}^T\mu_e\mathbf{J} + T_i^{\mathrm{tr}} \tag{7}$$

Here the first two contributions constitute T_i^{vib} and are included in H_s for $i = j$. While the latter two constitute $T_i^{\mathrm{tor-rot}} + T_i^{\mathrm{tr}}$ and are included in H_b. With this division, our solute Hamiltonian contains the kinetic energy due to the small amplitude vibrations of a single MeOH molecule, while the kinetic energy due to the torsions, rotations, and translations of all the molecules are included in the bath Hamiltonian.

In this separation, the torsional motion is included in the bath. We expect that the motion of the torsion is more strongly coupled to the surrounding molecules than it is to the vibrations of the same molecule. Moreover, in LT theory the bath degrees of freedom are treated classically, and since the torsion frequency is low, a classical treatment is reasonable.

We have made two approximations in the derivation of the kinetic energy. First, the vibrational kinetic energy of the $N-1$ bath MeOH molecules is set to zero. This is equivalent to ignoring intermolecular vibration−vibration transitions in the early stage of the relaxation. Previous studies that have compared rates with and without this approximation find that it is generally valid.[33,43] Moreover, as discussed above, Iwaki and Dlott see no heating of the bath on the time scale of the initial relaxation out of the OH stretch.[23] The second reason for making this approximation is computational. Since the bath consists of N molecules each with rotational, torsional, and translational degrees of freedom, any one molecule serves equally well as the solute molecule. As such, in an MD simulation we can follow all molecules at the same time and average rather than following a single trajectory for a long time.

The second approximation is neglecting Coriolis coupling. Lawrence and Skinner[34] have shown that while Coriolis coupling has essentially no effect on the initial rate, this is due to a fortuitous cancellation of potential−Coriolis and Coriolis−Coriolis coupling terms each of which contributes almost 30% to the lifetime of the OH stretch in HOD relaxation. Since this coupling scales with the components of the inverse moment of inertia of the molecule roughly perpendicular to the HOD plane in water or COH plane in MeOH,we have neglected the coupling here.

To express the potential in a form analogous to that of eq 3, i.e.,

$$U = U_s + U_b + V \tag{8}$$

we begin by writing U as a sum of two contributions

$$U(\mathbf{x}) = U_j^{\mathrm{mol}}(\mathbf{Q},\tau) + W(\mathbf{b},\mathbf{Q},\tau) \tag{9}$$

where $\mathbf{Q}$ are the normal coordinates of the *j*th molecule, and τ is the torsional variable. With the special role that τ plays in the molecular potential energy, we are explicitly noting it in the form of the potential even though it will always be considered a bath degree of freedom. As such, we could have included τ in the vector $\mathbf{b}$. For the present study, $U_j^{\mathrm{mol}}(\mathbf{Q},\tau)$ is chosen to be the gas-phase molecular MeOH potential. The remaining term W includes all other interactions.

The vibration−torsion potential is expressed as

$$U_j^{\mathrm{mol}}(\mathbf{Q},\tau) = U^0 + U^{3c}\cos(3\tau) + U^{3s}\sin(3\tau) \tag{10}$$

where the Fourier expansion coefficients are functions of the normal coordinates. In contrast to the usual approach where the normal coordinates are defined by diagonalizing the **FG** matrix at each value of the torsional coordinate and where the instantaneous equilibrium configuration is a function of τ, we diagonalize the $\bar{\mathbf{F}}\mathbf{G}$ matrix where $\bar{\mathbf{F}}$ is the torsionally averaged force constant matrix defined with respect to an equilibrium configuration that reflects the 3-fold symmetry of the molecule. While this separation increases vibration−torsion coupling, it has several advantages. In implementing LT theory, it is necessary to calculate the forces along the normal modes. To do so requires that one transforms from space-fixed forces to body-fixed forces and finally to normal modes. This second transformation is a function of the torsional coordinate, since our displacement coordinates are defined with respect to a body-fixed frame that depends on the torsional coordinate as well as the three Euler angles. The torsional dependence of the second transformation is relatively simple if we assume a torsionally averaged force constant matrix. The advantage of using torsionally averaged bond lengths and angles is that the rotation−torsion motion included in the molecular dynamics simulation is that of a rigid-twister where bond lengths and angles do not have to be readjusted at each value of the torsional coordinate.

The gas-phase contribution to the potential is written as

$$U_j^{\mathrm{mol}}(\mathbf{Q},\tau) = U^0 + U_e^{3c}\cos(3\tau) + [U^{3c} - U_e^{3c}]\cos(3\tau) + U^{3s}\sin(3\tau), \tag{11}$$

where the subscript e denotes evaluation of the Fourier coefficient at the equilibrium value of the normal coordinates. Combining eqs 9 and 11, we can now write U as a sum of three contributions. They are

$$U_s' = U^0$$

$$U_b = U_e^{3c}\cos(3\tau) + W(\mathbf{b},\mathbf{Q}=\mathbf{0},\tau)$$

$$V' = [U^{3c} - U_e^{3c}]\cos(3\tau) + U^{3s}\sin(3\tau) + [W(\mathbf{b},\mathbf{Q},\tau) - W(\mathbf{b},\mathbf{Q}=\mathbf{0},\tau)] \quad (12)$$

With this partitioning U_s' is the torsionally averaged isolated molecule potential, U_b describes all potential interactions when the molecules are constrained to their equilibrium configurations, and the coupling V' includes all remaining terms. The normal mode functional dependence of the interaction term V' is obtained by expanding it in a Taylor series to second order. With the above partitioning there is no constant term in V'.

This partitioning can be refined by averaging V' of eq 12 over the bath coordinates to obtain $\langle V'\rangle$. This term contains linear and quadratic terms in the normal coordinates. Adding and subtracting $\langle V'\rangle$ from U_s' and V', respectively, gives

$$U_s = U_s' + \langle V'\rangle$$

$$V = V' - \langle V'\rangle \quad (13)$$

thus giving us the partitioning of eq 8. Here the solute potential includes the gas-phase potential plus additional terms due to the average forces acting on the molecule in the liquid environment.

B. Vibrational Calculation. The solution of the vibrational Hamiltonian closely follows that used in a recent gas-phase study of MeOH by Castillo and Sibert.[44] In both studies, Van Vleck perturbation theory is used to find a representation with reduced coupling among the vibrational degrees of freedom. Although the gas-phase study used curvilinear normal coordinates and this study uses rectilinear normal coordinates defined with respect to body-fixed frame that depends on the instantaneous torsional coordinate, the implementation of Van Vleck perturbation theory is essentially identical. The potential is the same to the order at which the perturbation theory is carried out. Since Van Vleck perturbation theory changes the vibrational representation, it is necessary to transform accordingly the solute contribution to the solute−solvent coupling V of eq 3. This transformation is straightforward and follows the approach used by Sibert and Rey.[33]

At each stage in Van Vleck perturbation theory, one has the option of whether to transform away a specific coupling term. Following Castillo and Sibert[44] we base this decision by stating that our final Hamiltonian is defined by two polyad quantum numbers

$$N_i = \sum_j M_{ij} n_j$$

where n_j is the vibrational quanta in mode j defined in Table 1 and where

$$\mathbf{M} = \begin{pmatrix} 6 & 6 & 3 & 2 & 2 & 6 & 3 & 2 \\ 6 & 6 & 3 & 3 & 3 & 6 & 3 & 2 \end{pmatrix}. \quad (14)$$

If a coupling term couples two states with either the same value of N_1 or N_2, then that coupling is *not* transformed away. The constants in **M** are chosen so that our final Hamiltonian has direct couplings to the important states in Figure 2 corresponding to $\Delta v = 2$, 3, and 4. The form of the Hamiltonian used in the gas-phase study[44] is slightly different. There calculations were carried out to fourth order, whereas here we obtain results at second order. We use second order since less accuracy is needed in the liquid-phase work. Although the Hamiltonian is not block-diagonal, the representation is good enough that the eigenvalues of the states relevant to relaxation out of the OH stretch can be converged with a basis of just 364 functions.

TABLE 2: MeOH Structure Parameters in Å and Degrees

r_{OH}	0.9557
r_{CO}	1.4247
r_{CH}	1.0950
∠COH	109.7
∠HCO	109.0

To calculate the gas-phase and liquid-phase energies, the potentials U_s' and U_s of eq 13 are used, respectively, with the exception that the gas-phase potential includes the second two terms in eq 10 averaged over the gas-phase ground-state torsional wave function.

C. MD Simulation. The classical dynamics were computed using a MD simulation. The classical equations of motion are propagated in time; if long enough trajectories are performed, the appropriate phase space should be sampled. In the current MD simulation, 108 MeOH molecules were placed in a simulation box at 300 K and at the appropriate density of 0.79 g/cm. The bond lengths and angles were held fixed via the SHAKE algorithm,[45] while the torsional motion was allowed to evolve in time according to a hindered 3-fold rotational barrier. Ewald periodic conditions[46] were used to compute the electrostatic forces. The geometric parameters for the MeOH, obtained from the equilibrium geometry of the torsionally averaged $\bar{\mathbf{F}}$ matrix, are given in Table 2.

The intermolecular potential is comprised of a Lennard-Jones and electrostatic point charges, which reasonably reproduce the MeOH radial distribution functions. The potential is that of Wang et al.[47] and is in fairly close agreement with the AMBER potential for MeOH.

The time step for propagation via the velocity Verlet algorithm was 0.2 fs with terms in the interaction calculated every 2 fs. After equilibration for 200 ps, a 200 ps production run was performed. A subsequent reequilibration and production run was performed to check the stability of the results. The largest difference of a state-to-state rate calculated via Landau−Teller theory between the first run and the average of the two runs was 0.0053 ps^{-1} for state $5_2 11_1$. The first derivatives were calculated analytically via a rotation from the lab-fixed simulation frame to the molecular fixed frame. The second derivatives were calculated via numerical differentiation of the first derivatives. The numerical derivatives were found to be stable over a relatively wide range of displacements.

Due to the finite time of the simulation run there are noise issues that include minor fluctuations in the long-time tails of the time correlation functions (TCF's). To reduce this noise and the associated noise in the Fourier Transform (FFT), we multiply the TCF with a Gaussian to ensure that its tail smoothly approaches zero at long times. Minor fluctuations still remain in the FFT, so to extract a rate at a frequency ω_{mn} we average 5 FFT points in a 5 cm^{-1} window around this frequency. One additional manipulation of the data is performed for the transitions that are larger than 1200 cm^{-1}. With the interactions calculated every 2 fs, the high frequency tail in the spectral density behaves incorrectly past approximately 1500 cm^{-1}. To calculate rates at transition energies larger than this, the high-frequency tail is fit to a single exponential between 1200 and 1500 cm^{-1}. Since there is no fast vibrational motion in the MD simulation, we expect the spectral density to approach zero rapidly, and the exponential fit provides a good description of the data over the frequency window mentioned.

D. Quantum Correction Factors. With the use of a quantum time correlation function, detailed balance is satisfied. However,

with the use of a classical TCF, that is not the case and the expectation that excitation is energetically unfavorable is not upheld. Thus, various quantum correction factors (QCF's) have been utilized to bridge the gap between the quantum and classical regimes. While several QCF's have been shown to be exact for certain model problems, in general there is no QCF that works for all cases. We utilize the Harmonic/Schoenfeld QCF

$$Q(\omega) = e^{\beta\hbar\omega/4}\left(\frac{\beta\hbar\omega}{1 - e^{-\beta\hbar\omega}}\right)^{1/2} \tag{15}$$

because it works well for multiphoton processes and has been successfully used in previous work.[48] While the effect of the QCF can be rather dramatic for processes that involve large changes in energy, with the number of states within a couple hundred wavenumbers one might expect that if those states dominate the relaxation pathway that the effect and choice of a QCF might make little difference in the overall rate.

E. Time-Dependent Perturbation Theory. We follow the approach of Sibert and Rey[33] and solve the time-dependent Schrödinger equation $H_s + V$ of eq 3. The bath contribution to V is treated as a time-dependent contribution. This approach does not allow for the classical bath to respond to changes in the solute, and as such is more approximate than the mean field approach used by Terashima et al.[49] to describe population relaxation of CN^{-1} in an aqueous solution. In both approaches, one calculates single molecule population transfer between various states and then ensemble averages many single molecule results in order to compare to experiment or LT results.

An advantage of the TD approach is that it allows one to include the solvent-induced frequency shifts. When the results for chloroform were ensemble average, the average relaxation for the CH stretch was found to be in close agreement with LT theory.[33] There, however, the solvent-induced frequency shifts were relatively small. Here, this is not the case.

In its matrix form, the TD equation takes the form

$$i\hbar\dot{\mathbf{c}} = [\mathbf{H}_s + \mathbf{V}]\mathbf{c} \tag{16}$$

Sibert and Rey[33] assumed unit probability in the initially prepared vibrational state. This approach cannot explain the enhancement of the bend population upon red shift of the excitation pulse. In general, if the energy fluctuations are slow enough, this opens up the possibility of observing frequency-dependent rates of VER.[50] Lawrence and Skinner[51] developed a theory for frequency-dependent rates based on calculating rates for specific sub-ensembles of molecules identified by an energy mismatch. The frequency-dependent rates were calculated using time-dependent methods assuming static values of this mismatch.

We have not used that approach here as the effects of the fluctuations can be expected to be more acute for MeOH than they are for HOD. For the nearly degenerate $\Delta v = 4$ states of MeOH, the relative size of the fluctuations compared to the average separation is much greater than that found in HOD. For this reason, we include the frequency fluctuations dynamically by including the diagonal contributions to eq 16 and by incorporating an excitation laser pulse in the TD calculation. The laser excitation is explicitly included by assuming that population is initially in the ground state, the dipole moment operator is linear in Q_1 the normal coordinate of the OH stretch, and the time dependence of the laser field is given by

$$E(t) = E_o \exp[-(t - t_o)^2/T^2]\cos(2\pi c\omega_L t) \tag{17}$$

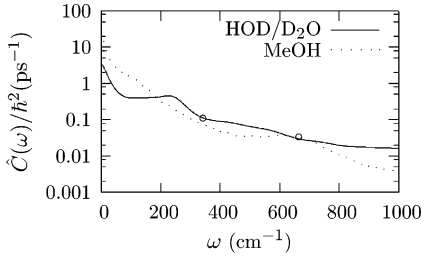

Figure 3. Comparison of $\hat{C}(\omega)/\hbar^2$ [cf. eq 2] for relaxation from the OH fundamental to the OH bend overtone for HOD/D_2O and methanol as a function of energy separation. The former data is from Lawrence and Skinner.[34] The circles correspond to the separations ω_{mn} used by that study and in the current work.

where c is the speed of light and the parameters t_o, T, E_o, and ω_L define the laser pulse.

IV. Results and Discussion

This section is subdivided as follows. We begin by presenting the vibrational energies as calculated using the methods described above. The vibrational energies are compared to experiment. We then present state-to-state rates calculated via LT theory and subsequently via TD theory. The TD results are compared to the LT results, and the key differences are highlighted. Finally, both LT and TD results are compared to experiment.

A. Vibrational Energies. In Table 1, we list both the harmonic and fundamental frequencies obtained from the perturbative calculations. The resulting calculated gas-phase energies qualitatively agree with experiment, although one calculated energy differs by 30 cm^{-1}. This agreement is satisfactory considering that the gas-phase potential is ab initio and is torsionally averaged assuming the torsion is in its ground state.

The liquid-phase results show greater disparities with experiment, particularly for the OH bond where the hydrogen bonding leads to a significant red shift in the liquid. Our solvent averaged potential U_s of eq 13 predicts a shift of 101 cm^{-1} compared to the actual shift of 238 cm^{-1}. This is an indication that the average solvent forces along the OH stretch coordinate in the MD simulation are weaker than those of the true liquid.

To bring our results into better agreement with experiment, we decreased the harmonic frequencies of the ν(OH) and ν(CO) modes by 173.5 and 20.0 cm^{-1}, respectively. The ν(CO) frequency was also adjusted because of its important contribution to the relaxation. The resulting energies are shown in Table 1. The agreement is now good with the exception of the δ_a(CH) fundamental, which is still about 50 cm^{-1} too low in energy. As will be shown, this state is not as important a vibration in the relaxation pathway, and hence it has not been adjusted.

B. Landau−Teller Rates. Landau Teller rates depend on the spectral density. In Figure 3, we present the spectral density for the transition from the ν(OH) to the δ(OH) overtone for our methanol system and for the HOD/D_2O system of Lawrence and Skinner.[34] There are features that are common in both works. There is a low-frequency bump ~200 cm^{-1} which roughly corresponds to a hydrogen bond stretch. Since MeOH is heavier, this motion is lower in energy. There is a second bump, which is not quite as noticeable for HOD on this scale, around 600 cm^{-1} which corresponds to an OH librational motion. For MeOH, the bump is slightly blue-shifted and also corresponds to librational motion. This motion is more correctly described has hydrogen-bond constrained libration about the CO

TABLE 3: Landau-Teller Results both with and without the Quantum Correction Factor for States with Lifetimes τ_c's less than 500 ps (States are listed in order of decreasing ω_{mn}, the energy difference (in cm^{-1}) between the OH-stretch fundamental at 3400 cm^{-1} and the state in question.)

		no QCF		with QCF	
state	ω_{mn}	rate/ps^{-1}	τ_c/ps	rate/ps^{-1}	τ_c/ps
5_2	1347.8	0.0049	202.94	0.0622	16.09
4_15_1	999.3	0.0077	130.52	0.0552	18.13
4_2	665.3	0.0336	29.78	0.1348	7.42
3_110_1	456.6	0.0042	237.95	0.0113	88.21
3_110_1	424.7	0.0046	217.34	0.0116	85.86
6_1	395.6	0.0039	253.75	0.0094	106.30
5_3	345.1	0.0093	106.96	0.0201	49.70
5_28_1	249.5	0.0330	30.27	0.0581	17.21
5_211_1	191.6	0.0447	22.40	0.0693	14.44
5_18_2	153.6	0.0027	375.58	0.0038	263.45
8_3	56.8	0.0094	106.61	0.0107	93.26
5_111_2	40.3	0.0036	279.08	0.0039	253.72
8_211_1	−4.9	0.0023	434.80	0.0023	439.94
4_15_2	−5.5	20.8014	0.05	20.5286	0.05
8_111_2	−60.4	0.0021	465.47	0.0019	538.36
$4_15_18_1$	−97.9	0.0498	20.06	0.0393	25.45
3_15_2	−108.1	0.0288	34.68	0.0222	45.11
5_27_1	−130.4	0.0150	66.74	0.0109	91.76
5_210_1	−133.7	0.0197	50.64	0.0142	70.20
$4_15_111_1$	−165.2	0.0238	42.03	0.0158	63.10
4_18_2	−191.6	0.0062	160.14	0.0039	257.11
4_25_1	−339.0	0.0117	85.64	0.0049	202.42
$3\,4_15_1$	−454.2	0.0107	93.35	0.0033	302.40
2_15_1	−475.7	0.0050	200.31	0.0015	689.00
$4_15_110_1$	−484.0	0.0056	176.99	0.0016	623.04
4_157_1	−484.3	0.0034	291.47	0.0010	1026.92
listed		21.1473	0.05	21.1018	0.05
total		21.1691	0.05	21.1623	0.05
listed w/o 4_15_2		0.3459	2.89	0.5732	1.74
total w/o 4_15_2		0.3677	2.72	0.6337	1.58

bond.[52] One can see that for most of the frequency range, the HOD rate is faster. There is a minor difference between the methods used to calculate the two spectra, our spectrum was calculated with the Fast Fourier Transform algorithm,[53] while the HOD spectrum was computed using the Wiener-Khintchine theorem with Hanning window.[53,54] The resulting HOD spectrum has slightly less noise than the MeOH spectrum.

We calculated transition rates out of the ν(OH) eigenstate to all eigenstates under 4000 cm^{-1}. In Table 3, we report only state-to-state rates that have time constants τ_c's less than 500 ps without a QCF. There are two obvious features of this table. First, there is only one $\Delta v = 2$ and six $\Delta v = 3$ transitions; the remaining are 19 $\Delta v = 4$ transitions. Second, the 4_15_2 state, which is nearly resonant in energy with the ν(OH) at 3400 cm^{-1} has a rate 3 orders of magnitude faster than any other rate.

We have previously commented on the expected order of state coupling to the various tiers in MeOH, so it is a little surprising that the relaxation pathway is dominated by the $\Delta v = 4$ tier, not only in quantity but also in magnitude. In fact the only state with both $\Delta v < 4$ and $\tau_c < 100$ ps is the 4_2 state, this being the dominant acceptor state in HOD/D_2O.[31,34] Within the $\Delta v = 4$ tier, there are many states that contribute to the OH decay. We can rationalize some of the trends by recognizing that the 4_15_2 state plays a special role. Relaxation to this state is orders of magnitude faster than any other state due a combination of weak coupling and its near degeneracy with the OH fundamental. This degeneracy causes the OH fundamental to have some 4_15_2 zero-order character via state mixing. This mixing leads to the secondary effect of stronger than expected coupling between the OH fundamental and states with either $4_15_1X_1$ or $4_05_2X_1$, where X is any of the low-frequency modes.

The fast rate to the 4_15_2 state is an artifact of using an average energy difference between two states in calculating the LT rate. In reality, there are large energy fluctuations as functions of time. We shall see in the next subsection that the time-dependent approach allows us to include these fluctuations in a natural way, and that the fluctuations essentially unmix the states. As such, we will not attempt to "patch up" LT theory by decoupling the mixed states. Instead we simply report lifetimes with and without inclusion of the 4_15_2 state in the total transition rate. The resulting time without this state is 2.72 ps, which is slower than observed in the ID experiment, but not unreasonable considering the many approximations that have been made along the way.

In the final two columns of Table 3, we include the Harmonic/Schoenfeld QCF. This quantum correction factor increases the rate to states with energies below 3400 cm^{-1} and decreases the rate to states with energies above 3400 cm^{-1}. We see that with the QCF the δ(OH) overtone rate increases by a factor of 4 to become the dominate state in the relaxation manifold. This assumes that we continue to neglect the 4_15_2 state. The increase for the 4_2 state contrasts to the corresponding overall rate increase of a modest factor of 1.6. Evidently, the competing flow of probability to nearly degenerate states with smaller correction factors tempers the overall effect of the QCF.

C. Time-Dependent Rates. In this subsection, we compare Landau−Teller and time-dependent results for the OH relaxation. Sibert and Rey[33] carried out a similar comparison for CH relaxation of chloroform and found that the ensemble averaged time-dependent results were statistically equivalent to the LT results. Lawrence and Skinner[43] made similar comparisons for the OH relaxation in HOD and also found little difference in the OH relaxation rate, although differences were found for other transitions with faster LT rates.

We are motivated to pursue a similar comparison here, since Figure 2 suggests and Table 3 predicts that there are near resonant states, i.e., states with small values of ω_{mn} that contribute to the relaxation. This separation, which is the average separation, is comparable to the size of the instantaneous energy level fluctuations

$$\Delta\omega = \omega + \Delta\omega_s \tag{18}$$

where $\Delta\omega_s$ is the contribution relative to the average. The subscripts m and n are omitted, since it is clear to which states we refer. The size of $\Delta\omega_s$ changes significantly as the OH forms and breaks hydrogen bonds. These fluctuations are not included in LT theory.

These fluctuations are calculated via

$$\Delta\omega_s = \langle m|V/hc|m\rangle - \langle n|V/hc|n\rangle. \tag{19}$$

Here m and n are the initial and final states, respectively, and V is the solvent-bath coupling of eq 13.

We begin by considering a 3-state model that includes the ground state, the 1_1 OH fundamental, and the 4_2 OH bend overtone. Figure 4 shows that the time-dependent results are about a factor of 2 faster than the corresponding LT results without the quantum correction factor. There are several possible reasons for this difference, one of them being the instantaneous fluctuations of the energy levels. To verify that these fluctuations lead to the faster rates, we recalculated the time-dependent rates, reducing by a factor of 15 the magnitudes of those terms that

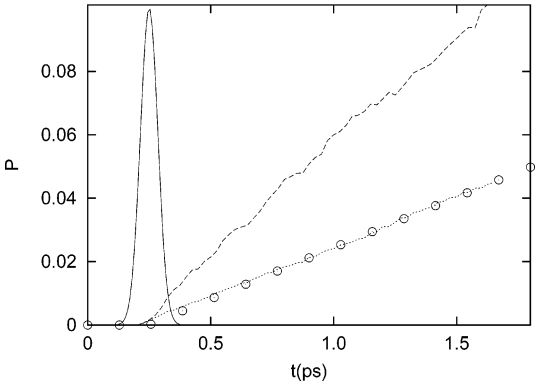

Figure 4. Relaxation results for the three-state time-dependent calculation that includes the ground state, the 1_1 state, and the 4_2 state. The time-dependent laser field, given by eq 17 has $t_o = 0.25$ ps, $T = 0.05$ ps, and $\omega_L = 3400$ cm^{-1}. The temporal width corresponds to $\Delta\omega = 360$ cm^{-1}. The near impulsive pulse, which is significantly narrower (in time) than that used by Iwaki and Dlott, allows easier comparison to LT results. The curve (- - -) is the rate of probability flow from the OH fundamental to the COH overtone. The curve (...) is the rate of probability flow between the same states but the diagonal couplings have been reduced by a factor of 15. The points correspond to the Landau−Teller lifetime result of 29.8 ps of Table 4.

TABLE 4: MD Results for the Average Force along OH-Stretch Coordinate Normalized with Respect to the Wang et al.[47] Potential for Four Choices of Charges (in electrons) (Dipole moments (in Debye) and angles θ (in degrees) between the dipole moment and the OH bond are also listed.)

q_O	q_{H_0}	μ	θ	$\langle F \rangle$
−0.5	0.3	1.92	67.3	0.29
−0.6	0.4	2.14	55.9	1.00
−0.7	0.5	2.43	46.9	1.99
−0.8	0.6	2.76	39.9	3.61

lead to the fluctuations, these being the diagonal coupling terms. These rate results, also shown in Figure 4, are in excellent agreement with LT theory. We conclude that the difference between LT and TD rates is due to the energy fluctuations being neglected in the former.

To quantify the importance of these fluctuations, we write the time-dependent rate constant for the probability of going from the OH stretch to the bend overtone as

$$k^{TD} = \int_{-\infty}^{\infty} d\Delta\omega_s \, P(\Delta\omega_s) \, k^{TD}(\Delta\omega_s) \qquad (20)$$

where $P(\Delta\omega_s)$ is the probability of an instantaneous energy separation $\omega + \Delta\omega_s$, and $k^{TD}(\Delta\omega_s)$ is the rate at that separation. The procedure can be compared to an energy-weighted LT rate also obtained using eq 20, but replacing $k^{TD}(\Delta\omega_s)$ with the analogous LT rate $k^{LT}(\Delta\omega_s)$. The rate $k^{TD}(\Delta\omega_s)$ is obtained in the TD calculation obtained by evaluating the appropriate $\dot{c}_n$ of eq 16 every 0.025 ps and binning the results as a function of $\Delta\omega_s$. The analogous LT rate is obtained by replacing ω_{mn} with $\Delta\omega$ in eq 1. These rates are plotted as points and a thick line, respectively, in Figure 5. Also shown is the double humped plot of $P(\Delta\omega_s)$ versus $\Delta\omega_s$.

Strikingly, one finds that over most of the $\Delta\omega_s$ range the LT results and time-dependent results are in good agreement, albeit with large uncertainties. This is seen most clearly in the inset of the figure. Only for small separations (large negative $\Delta\omega_s$ values) are time-dependent rates substantially faster. The time-dependent rate in the bin centered at $\Delta\omega_s = -380$ cm^{-1} is 1.24 ps^{-1} compared to the LT rate of 0.12 ps^{-1}. Although not shown in the figure, the rate for the bins centered at −420 and −460 cm^{-1} are 2.67 and 3.47 ps^{-1}, respectively. The LT rate for this latter bin is only 0.29 ps^{-1}.

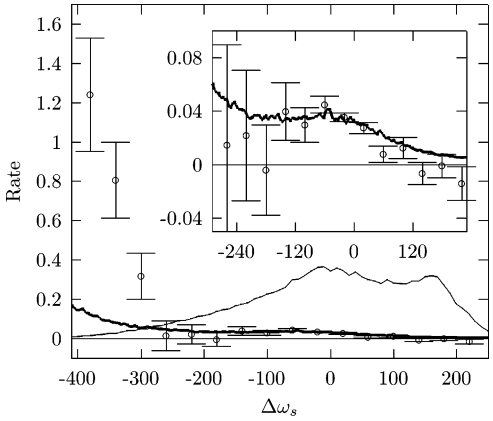

Figure 5. Rate $k^{TD}(\Delta\omega_s)$ is binned and plotted as points (o) as a function of $\Delta\omega_s$ [cf. eq 20] where $k^{TD}(\Delta\omega_s)$ is rate (ps^{-1}) of going from the 1_1 OH stretch fundamental to the 4_2 bend overtone evaluated at $\Delta\omega_s$. Here $\Delta\omega = 665.3 + \Delta\omega_s$ is the instantaneous energy difference between these states. The error bars are $\pm\sigma/\sqrt{N}$ where N is the number of data points per bin and σ is the standard deviation. The rate is calculated as the time rate of change of probability of being in the 4_2 state as calculated using the three-state, time-dependent model discussed in the text. The rate dramatically increases as the separation decreases. Also shown are the Landau−Teller rate constant $k^{LT}(\Delta\omega_s)$ (thick line) as a function of $\Delta\omega_s$ and the frequency distribution $P(\Delta\omega_s)$ (thin line) plotted as a function of $\Delta\omega_s$ (in cm^{-1}). The latter curve, which is double humped, was obtained using eq 19. The normalization is arbitrary.

The averaged LT result yields a lifetime of 31.8 ps; this is essentially identical to the lifetime of 29.8 ps given in Table 3. Therefore, the factor of 2 ratio between averaged TD and LT rates is due to a few trajectories in the tail of the energy separation distribution that is shown in Figure 5. In contrast to the TD result, the weighted LT result does not include the correlation between large negative values of $\Delta\omega_s$ and large off-diagonal forces that lead to population transfer. Moreover, even though $\Delta\omega$ never reaches zero, a separation of $\Delta\omega \approx 200$ cm^{-1} is sufficiently small that we can conjecture that the accepting bath mode involves a hydrogen bond motion and not the torsional motion.

We now consider the results of a three-state model that includes the ground state, the 1_1 state, and the 4_15_2 state, this latter state having the fastest LT rate in Table 3. Given that $\omega = -5.54$, the fast rate is not surprising. From a time-dependent perspective this near resonant state will undergo repeated avoided crossings with the 1_1 state as $\Delta\omega$ fluctuates between positive and negative values as a function of time. The results of the TD calculation are given in Figure 6. The dashed line results show rapid energy flow during the excitation pulse followed by a slower increase. This initial rise is a consequence of the 4_15_2 eigenstate having some 1_1 zero-order character; the rapid flow is due to direct coupling via the laser field with the ground state. This flow would occur even in the limit that the dynamic solvent coupling V is zero.

A more direct comparison to experiment would be to calculate the probability of observing anti-Stokes transitions as a function of time. If we make the assumption that the transition operators are linear in the normal mode coordinates giving the $\Delta v = 1$ normal mode selection rule, then the relevant quantity to calculate theoretically is the probability of being in either the zero-order 1_1 or 4_15_2 state as a function of time. Energetics is not an issue, since both these states have essentially the same energy.

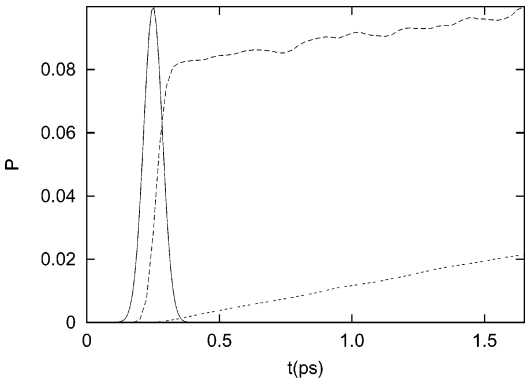

Figure 6. The relaxation results for the three-state time-dependent calculation that includes the ground, the 1_1, and the 4_15_2 eigenstates. The Gaussian curve is the amplitude of the time-dependent laser excitation pulse. The curve (- - -) is the rate of probability flow into the 4_15_2 state. Due to the near degeneracy with the OH fundamental and the resulting state mixing, this state carries oscillator strength, and hence rapid probability flow appears during the laser excitation. The curve (...) results if we take the appropriate admixtures of the above eigenstates to form states that closely resemble zero-order 1_1 and 4_15_2 states. The observed lifetime of 66 ps is significantly slower than the Landau−Teller lifetime of 0.05 ps given in Table 4. The laser pulse is the same as in Figure 4.

The present situation is one with substantial mixing between the zero-order states, due to the near degeneracy. It is particulary easy to calculate the probability of being in a zero-order state, since this is an isolated resonance, and one can take linear combinations of the two eigenstates in question to form approximations to the zero-order states. Diagonalizing the full molecular Hamiltonian to obtain the eigenstates of H_s of eq 3, we find that the two eigenstates used in the above three-state model have the following description

$$|1_1\rangle = 0.93|1_1\rangle^o - 0.27|4_15_2\rangle^o + \cdots$$

$$|4_15_2\rangle = 0.28|1_1\rangle^o + 0.93|4_15_2\rangle^o + \cdots \qquad (21)$$

where $|1_1\rangle^o$ and $|4_15_2\rangle^o$ are the basis states of the zero-order contribution of H_s after applying Van Vleck perturbation theory. (Note, these zero-order states look almost the same before and after the application of Van Vleck perturbation theory, since we are not removing any resonant interaction with the perturbation theory.) We take linear combinations of the above two eigenstates to obtain good descriptions of the zero-order states, since 95% of the eigenfunctions are accounted for by these two zero-order states. Having already carried out the TD calculation in the eigenstate representation, we know the $c_i(t)$ values corresponding to the two eigenstates. We take the linear combinations of these values (including the usual $\exp[iE_jt/\hbar]$ factors, where E_j are the eigenvalues of H_s) to calculate the probabilities of being in the decoupled states. Following this approach, we obtain the dotted line result in Figure 6. Not surprisingly, the zero-order OH stretch state is the bright state; it is the state that is initially excited. The corresponding lifetime for the zero-order OH stretch is 66 ps, which is in stark contrast to the 0.05 ps LT result for the lifetime of the associated eigenstates. Even with multiple avoided crossings, the $|4_15_2\rangle^o$ state only plays a minor role in the overall relaxation process. Finally, we note that the transformation of representations has essentially no effect on the rate of probability change between states after the laser field has been shut off since the lines in Figure 6 run parallel to each other after 0.5 ps.

In Figure 7 a, we show the results of 7 different three-state models. Each result was obtained using the ground state, the 1_1 state, and a nearby state whose identity is given in the key of the figure. The states in the key are listed in order of decreasing rates as one goes down the list. The TD (LT) lifetimes corresponding to each of these states is 9.4 (30.3), 13.9 (29.8), 14.9 (20.1), 38.0 (160.1), 65.9 (0.05), 156 (616), and 425 (807) ps, respectively. The differences between the LT and TD results arise for reasons that are similar to those invoked above in the discussion of flow of probability into the bend overtone Figure 4. The correlation plots for these states are similar to that of Figure 5. The 4_15_2 state is an exception. The reason for its greatly reduced TD rate has been explained above.

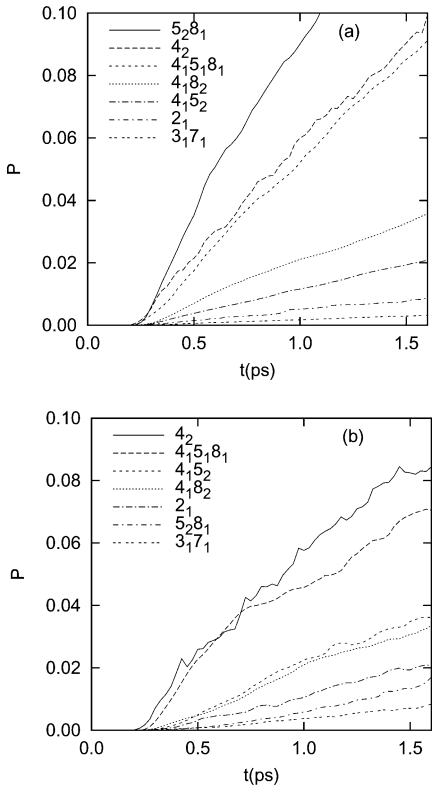

Figure 7. (a) The relaxation results for the *uncoupled* 9 state time-dependent calculation discussed in the text. The ordering in the figure key corresponds to the order of the importance of the 7 accepting states, the greatest flow occurring for the 5_28_1 states. Plot (b) is the same as plot (a) with the exception that the states are fully coupled. As discussed in the text, the role of the 5_28_1 is greatly diminished in the fully coupled model. The laser pulse is the same as in Figure 4.

In Figure 7b, we show results analogous to those of Figure 7a. The difference is that in the former calculation all states with the exception of the ground state are coupled to each other via the solvent interactions. The results are qualitatively similar. The most notable exception is that the role of the 5_28_1 state is significantly reduced from that of the uncoupled model. In the fully coupled model, we have taken the appropriate linear combinations of the 1_1 state and the 4_15_2 state as described above in explaining Figure 6. The dynamical fluctuations lead to a decoupling of these two zero-order states with the new result that the 5_28_1 now plays a less significant role. In the LT results discussed above and the three-state TD model, the bright state has some 4_15_2 character. This component allows coupling of the bright state to the 5_28_1 state via $\Delta v = 2$ transition.

Motivated by the experiment of Iwaki and Dlott,[23] we have repeated the nine-state calculation using laser pump frequencies of 3250 cm^{-1} and 3400 cm^{-1}. Here we use laser pulses that have much narrower spectral widths than were used above. This 50 cm^{-1} width is comparable to the 35 cm^{-1} value of the excitation pulse used in the experiment. Compared to the shorter

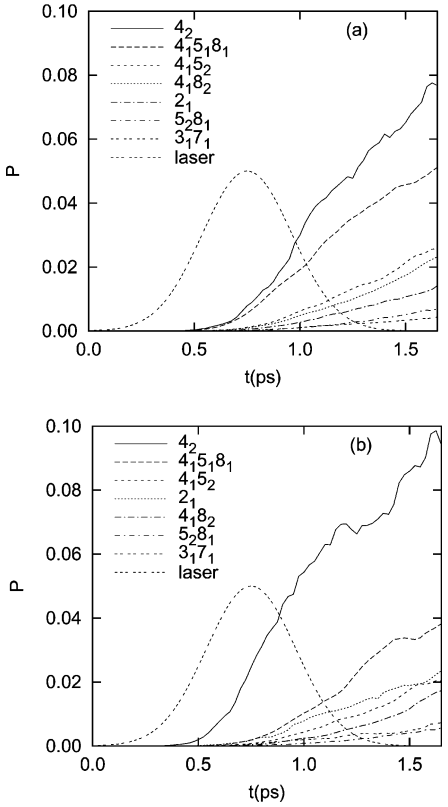

Figure 8. Results for the 9 state model as Figure 4b but with different excitation pulse. Laser frequencies in (a) and (b) are centered at $\omega_L =$ 3400 and 3250 cm^{-1}, respectively. The temporal width, given by $T =$ 0.3 ps in eq 17, yields a spectral fwhm of 50 cm^{-1}. The probability flow into the OH bend overtone is significantly enhanced compared to the other states upon this lowering of the excitation frequency.

temporal pulses, we are now able to probe molecules belonging to different sub-ensembles characterized by absorption frequencies. The results, shown in Figure 8, indicate that the lower-frequency pump excitation increases dramatically the role of the OH bending degree of freedom and to a lesser extent that of the CH stretch. In fact, the bend appears to turn on with the excitation pulse, suggesting that this state appears to have more bright character when excited at the lower frequency. This behavior has been observed experimentally by Iwaki and Dlott.[23] Finally we note that the difference between Figure 7b and Figure 8a is more modest. This difference is due to the change in the temporal width of the pulse maintaining $\omega_L = 3400$ cm^{-1} for both.

D. Comparison of LT and TD Theories with Experiment. To obtain the lifetime of the OH stretch using the TD method, we have performed a TD calculation that includes the ground state and all the eigenstates in the energy window between 2550 and 3626 cm^{-1}, this range being sufficient to include all the states that are predicted to be important by LT theory. We have also deconvoluted the 1_1 and $4_1 5_2$ states as described in the caption to Figure 6. We calculate a lifetime of 3.1 ps using the ultrashort laser pulse of Figure 4. This lifetime compares well to the LT results with and without the quantum correction factors of 1.6 and 2.7 ps, respectively. Clearly there is a cancellation of differences when summing the state-to-state rates. One might have expected that the TD result would be faster, since the state-by-state comparisons showed that the TD rates were faster. These faster rates, however, are offset by the reduced TD rates to states that have two quanta in the CO stretch. This effect is clearly seen in the comparison of Figure 7, parts a and b.

When considering where the energy goes after the initial excitation, some care must be taken when comparing with the experiments. The experiments do not actually measure the probability of being in a given eigenstate as a function of time. The experimental results of Figure 1 show population in the various modes as functions of time. To obtain these populations, Iwaki and Dlott[23] converted the anti-Stokes transients into populations. Since there is spectral overlap of the transitions, they had to deconvolute the overlapping transitions by assuming Voigt line shapes for each of the individual transitions. Finally, they convert intensities of the transients into populations being sure to distinguish $2\nu_j \rightarrow \nu_j$ from $\nu_j \rightarrow$ *ground* transitions.

On the theoretical side, we are at present limited to short time dynamics, and hence cannot compare to the full time scale of experimental results. The TD calculation does not adequately treat relaxation processes where the solute molecule loses vibrational quanta directly to the bath degrees of freedom. Large quantum corrections factors are needed, and it is not clear how to include these in the TD approach. One can look at the longer time dynamics with the LT approach by constructing a full master equation of rate constants between all the levels,[43] but given the high density of states this is beyond the scope of the present paper. Here, we look only at the short time dynamics where there is rapid redistribution of energy within the solute so that solute energy is maintained relatively constant.

To compare our results with the short time dynamics of Iwaki and Dlott[23] we map the populations of our eigenstates used in both the LT and TD calculation onto mode populations by assuming the modes are unmixed and the identity of the mode is determined by the leading coefficient in the basis set expansion. We then follow the standard procedure[14,23] of assuming the overtones are observed via the $2\nu_j \rightarrow \nu_j$ transitions with twice the amplitude of the $\nu_j \rightarrow$ *ground* transition; combination bands $\nu_i + \nu_j$ contribute to both the $\nu_i \rightarrow$ *ground* and $\nu_j \rightarrow$ *ground* transitions. As such, our population is calculated as

$$\text{population}_j = \sum_{\mathbf{n}} P_{\mathbf{n}} n_j \qquad (22)$$

where $P_{\mathbf{n}}$ is the time-dependent probability of being in an eigenstate whose leading coefficient corresponds to the basis state $\mathbf{n} = \{n_1, n_2, \cdots n_{11}\}$. Since the $\rho(CH_3)$, $\nu_a(CH)$, and $\delta_a(CH)$ modes each includes two nearly degenerate vibrations and their populations cannot be frequency resolved,[23] we have summed the contributions of each of these modes to obtain the results of Figure 9.

Figures 9a and 9b show the TD and LT results, respectively. The TD results correspond to the 3400 laser excitation of Figure 4; the LT results do not include the quantum correction factors. These two approaches give relaxation times for the OH stretch that are nearly identical. All modes are excited to some extent in the first picosecond in both calculations. The δ(OH), ν(CO), and $\rho(CH_3)$ are the most active acceptor modes in both, and the ν_s(CH) and ν_a(CH) are populated the least. A notable difference is that the LT result has the ν(CO) stretch being the dominant acceptor mode, whereas the TD calculation has the δ(OH) and $\rho(CH_3)$ as the dominant acceptor modes. This difference can be understood in terms of the results of Figure 7 where one observes that the coupling of the states in (b) greatly diminished the importance of the $4_1 5_2$ state from that given in the uncoupled model results of (a). Other states with $4_1 5_1 X_1$ or $4_0 5_2 X_1$ will be similarly affected.

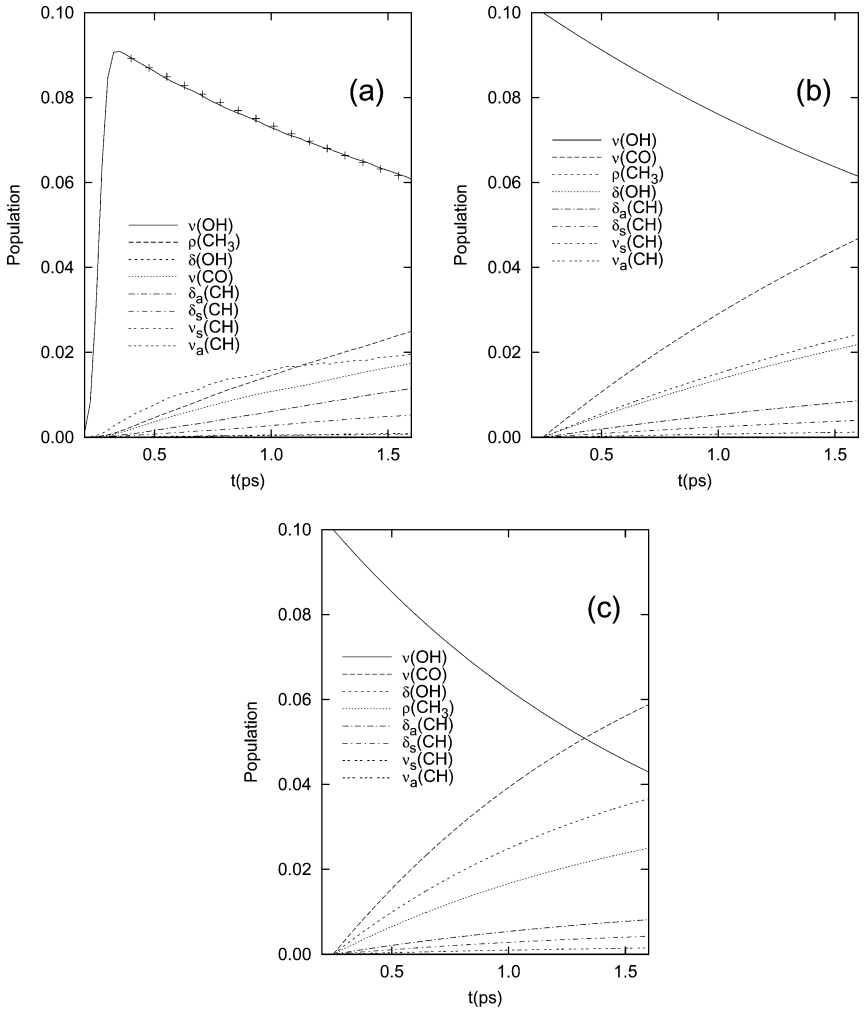

Figure 9. Plots of population in each of the spectrally distinct normal modes as a function of time. (a) TD results for laser excitation of 3400 cm^{-1} and an ultrafast temporal pulse of ≈0.1 ps, (b) LT results without the quantum correction, and (c) LT results with the quantum correction factor. The ordering in the figure keys corresponds to the ordering of the population in the modes after 1.6 ps. The points in (a) are exponential decay with a lifetime of 3.1 ps. This time is in close agreement with the 2.7 ps and 1.6 LT lifetimes with and without the quantum correction factor. The LT populations are scaled to aid comparison to TD results.

Figure 9c shows the LT result with the quantum correction. These results are consistent with Table 4. The shorter lifetime of 1.6 ps is mainly due to the faster rate of flow into the δ(OH) overtone.

In comparing our results to those of Iwaki and Dlott, we find that the relaxation rate of ν(OH) is at least a factor of two to three slower. In terms of where the energy goes, there is qualitative agreement. The lower-frequency modes are all more active than the ν_s(CH) and ν_a(CH). The time-dependent results and experiment show an enhancement upon decreasing the frequency of the OH excitation pulse.

Our results are slower than the 0−1 ps observed experimentally. While the experimental and theoretical difference between the lifetime of the ν(CH) in $CHCl_3$[33] is small, strongly interacting hydrogen bonding systems (such as our work on MeOH and previous HOD[31,34] studies) underestimate the rate of relaxation. One of the fundamental shortcomings of our calculations is the form of the potential we used in the classical MD simulations; it does not include polarization.

The importance of inductive effects has long been realized for line shapes of far-infrared spectra[55] and dielectric relaxation.[56] The dipole moment of 1.7 D in the gas phase is substantially lower that the average liquid-phase value of 2.49 D. Recent work in condensed phase ab-initio quantum dynamics has shed new light on the electrostatics of hydrogen bonding liquids. Handgraaf et al.[57] and Pagliai et al.[58] have performed Car-Parrinello molecular dynamics on MeOH and fully deuterated MeOH, respectively. They calculate O−O radial distribution functions that agree with experiment.[59,60] They also calculate average liquid dipole moment values of 2.54 D[57] and 2.64 D[58] which are in good agreement with experiment. Moreover the distribution of dipole moments is found to span 1.7 to 3.5 D. This latter result clearly indicates that the interaction of MeOH molecules is associated with dramatic charge rearrangement which cannot be reproduced by a static charge MD potential as has been utilized in this work and in HOD.[31,34]

The Wang et al.[47] intermolecular potential which we use has charges of −0.6 and 0.4 e on the oxygen and hydroxyl hydrogen sites, and this leads to a 2.14 D dipole moment per MeOH molecule which is similar to the 2.18 D dipole of TIP4P water. This dipole, however, is substantially less than the above-mentioned experimental and ab-initio MD values. The smaller value is the result of the MD potential parameters being fit in order to correctly predict pair correlation functions and equations of state. This value of the dipole moment leads to an O−O radial distribution function that agrees with experiment.[59,60]

In a preliminary investigation of the effects of altering the charges on MeOH, we performed several MD simulations with different charges on the oxygen and hydroxyl hydrogen; some

selected results are presented in Table 4. The final column in Table 4 shows the normalized force along the ν(OH) coordinate with respect to the Wang et al.[47] potential. While we have obviously greatly simplified the situation by only changing the hydroxyl atoms point charges, we can see that relatively modest changes in the charges and dipole moments lead to fairly large changes in the average force. As a means of comparison, the average force due to the 6/4 charges leads to a ν(OH) frequency of 3585 cm^{-1}, while the 7/5 charges, which lead to the correct dipole, nearly double the average force along ν(OH). This choice results in a frequency of 3483 cm^{-1} that is in much better agreement with the 3400 cm^{-1} center frequency of the experimental ν(OH) spectrum.

However, when we increase the charges (in units of electrons) on the oxygen and hydroxyl hydrogen from -0.6 and 0.4 to -0.7 and 0.5, respectively, and repeat the MD simulation, we find, not surprisingly, that there are corresponding structural changes. For example, the resulting O$-$O radial distribution function has a much narrower first inner peak than the corresponding experimental one. It is not clear to us that one can use fixed charges and fit both the average dipole and the O$-$O radial distribution function. Even though there are substantial shortcomings with the potential used in the MD simulation, the fact that we have qualitative agreement with all experimental observations leads us to have faith in our models even if we cannot reproduce quantitative results.

There is a clear need for the use of more sophisticated force fields. Sibert and Rey[33] included polarization affects with flexible molecules in the relaxation of chloroform. There the effects were found to be negligible. Future work will include extending such polarization models to treat hydrogen bonding in methanol.

V. Summary

The lifetime of the OH-stretch fundamental of liquid MeOH has been calculated using Landau$-$Teller theory (LT) and the time-dependent Schrödinger equation (TD). We find lifetimes of 2.7 and 3.1 ps for LT and TD, respectively. Application of the harmonic/Schofield quantum correction factor reduces the LT result from 2.7 to 1.6 ps, which is in fairly close agreement with the experimental result of 0$-$1 ps. Also in accord with experiment, we observe that all vibrational modes are excited in the initial intramolecular relaxation process and that the relaxation is sensitive to the frequency of the initial excitation pulse.

In contrast to the experiment, we determine directly state-to-state relaxation rates. We find that $\Delta\nu = 2$ processes, which allow for energy transfer from the OH-stretch to other vibrational fundamentals, do not contribute significantly to the relaxation of the OH fundamental. A combination of low coupling strength and/or large energy mismatches makes these pathways relatively unimportant. The $\Delta\nu = 3$ transitions are dominated by the OH bend overtone; this state has also been calculated to be the dominate energy-accepting state for HOD relaxation in D_2O.[31,34] However, unlike HOD, MeOH has $\Delta\nu = 4$ transitions that are nearly degenerate with the OH fundamental. The LT results indicate that $\Delta\nu = 4$ transitions dominate the relaxation without application of the quantum correction factor, but that $\Delta\nu = 3$ and $\Delta\nu = 4$ transitions contribute equally to the total rate with the quantum correction factor.

Although the LT and TD approaches lead to similar conclusions, there are some practical advantages to each. The advantage of using the LT approach is that the use of a quantum correction factor is straightforward, even if the choice of the quantum correction factor is not. There are two advantages to the TD calculation: the ability to naturally treat the solvent-induced energy fluctuations that can lead to avoided curve crossings, and the ability to selectively probe subsets of the molecules by including a pump laser in the calculation. Although the LT and TD rates are similar, there are notable differences in the state-to-state rates. We have discussed several instances where the two methods give different results in order to highlight the approximations of the methods.

Acknowledgment. This material is based upon work supported in part by the National Science Foundation under Grant No. CHE0315243 and the Vilas Trust of the University of Wisconsin. Parts of this work were carried out at the UW Chemistry Parallel computing center funded by NSF Grant No. CHE0090916 and gifts from the Intel Corporation. The authors thank James Skinner and Christopher Lawrence for helpful conversations and Dana Dlott for permission to use Figure 1.

References and Notes

(1) Morresi, A.; Mariani, L.; Distefano, M. R.; Giorgini, M. G. *J. Raman Spectrosc.* **1995**, *26*, 179.
(2) Hynes, J. T.; Rey, R. In *Ultrafast Raman and Infrared Spectroscopy*; Fayer., M., Ed.; Marcel Dekker: New York, 2001.
(3) Dlott, D. D. *Chem. Phys.* **2001**, *266*, 149.
(4) Deák, J. C.; Iwaki, L. K.; Rhea, S. T.; Dlott, D. D. *J. Raman Spectrosc.* **2000**, *31*, 263.
(5) Nienhuys, H. K.; Woutersen, S.; van Santen, R. A.; Bakker, H. J. *J. Chem. Phys.* **1999**, *111*, 1494.
(6) Lock, A. J.; Bakker, H. J. *J. Chem. Phys.* **2002**, *117*, 1708.
(7) Deák, J. C.; Rhea, S. T.; Iwaki, L. K.; Dlott, D. D. *J. Phys. Chem. A* **2000**, *104*, 4866.
(8) Pakoulev, A.; Wang, Z. H.; Dlott, D. D. *Chem. Phys. Lett.* **2003**, *371*, 594.
(9) Zhong, Q.; Baronavski, A. P.; Owrutsky, J. C. *J. Chem. Phys.* **2003**, *118*, 1074.
(10) Wang, Z.; Pakoulev, A.; Dlott, D. D. *Science* **2002**, *296*, 2201.
(11) Heckscher, M. M.; Sheps, L.; Crim, F. F. *J. Chem. Phys.* **2002**, *117*, 8917.
(12) Bakker, H. J.; Planken, P. C. M.; Kuipers, L.; Lagendijk, A. *J. Chem. Phys.* **1991**, *94*, 1730.
(13) van den Broek, M.; Bakker, H. *J. Chem. Phys.* **2000**, *253*, 157.
(14) Graener, H.; Zurl, R.; Hofmann, M. *J. Phys. Chem. B* **1997**, *101*, 1745.
(15) Graener, H.; Patzlaff, T.; Kadarizman, N.; Seifert, G. *Chem. Phys. Lett.* **2001**, *348*, 403.
(16) Seifert, G.; Kadarisman, N. *Chem. Phys.* **2003**, *288*, 223.
(17) Elles, C. G.; Bingemann, D.; Heckscher, M. M.; Crim, F. F. *J. Chem. Phys.* **2003**, *118*, 5587.
(18) Levinger, N. E.; Davis, P. H.; Fayer, M. D. *J. Chem. Phys.* **2001**, *115*, 9352.
(19) Laenen, R.; Simeonidis, K. *Chem. Phys. Lett.* **1999**, *299*, 589.
(20) Seifert, G.; Patzlaff, T.; Graener, H. *Chem. Phys. Lett.* **2001**, *333*, 248.
(21) Lim, M.; Hochstrasser, R. M. *J. Chem. Phys.* **2001**, *115*, 7629.
(22) Seifert, G.; Patzlaff, T.; Graener, H. *J. Mol. Liq.* **2003**, *102*, 227.
(23) Iwaki, L. K.; Dlott, D. D. *J. Phys. Chem. A* **2000**, *104*, 9101.
(24) Elles, C. G.; Cox, M. J.; Crim, F. F. Submitted.
(25) Yoo, H. S.; DeWitt, M. J.; Pate, B. H. *J. Phys. Chem. A*, submitted.
(26) Poulsen, J. A.; Rossky, P. J. *J. Chem. Phys.* **2001**, *115*, 8024.
(27) Qiang, S.; Geva, E. *J. Chem. Phys.* **2003**, *119*, 9030.
(28) Deng, Y.; Stratt, R. M. *J. Chem. Phys.* **2002**, *117*, 1735.
(29) Morita, A.; Kato, S. *J. Chem. Phys.* **1998**, *109*, 5511.
(30) Whitnell, R. M.; Wilson, K. R.; Hynes, J. T. *J. Chem. Phys.* **1992**, *96*, 5354.
(31) Rey, R.; Hynes, J. T. *J. Chem. Phys.* **1996**, *104*, 2356.
(32) Gnanakaran, S.; Hochstrasser, R. M. *J. Chem. Phys.* **1996**, *105*, 3486.
(33) Sibert, E. L.; Rey, R. *J. Chem. Phys.* **2002**, *116*, 237.
(34) Lawrence, C. P.; Skinner, J. L. *J. Chem. Phys.* **2002**, *117*, 5827.
(35) Gaffney, K. J.; Piletic, I. R.; Fayer, M. D. *J. Phys. Chem. A* **2002**, *106*, 9428.
(36) Laenen, R.; Gale, G. M.; Lascoux, N. *J. Phys. Chem. A* **1999**, *103*, 10708.
(37) Staib, A.; Hynes, J. T. *Chem. Phys. Lett.* **1993**, *204*, 197.
(38) Staib, A. *J. Chem. Phys.* **1998**, *108*, 4554.
(39) Oxtoby, D. W. *Annu. Rev. Phys. Chem.* **1981**, *32*, 77.

(40) Gussoni, G. D. M.; Hougen, J. T. *J. Mol. Spectrosc.* **1973**, *47*, 515.
(41) Szalay, V. *J. Mol. Spectrosc.* **1988**, *128*, 24.
(42) Hougen, J. *J. Mol. Spectrosc.* **1997**, *181*, 287.
(43) Lawrence, C. P.; Skinner, J. L. *J. Chem. Phys.* **2003**, *119*, 1623.
(44) Castillo-Chará, J.; Sibert, E. L. *J. Chem. Phys.* **2003**, *119*, 11671.
(45) Ciccotti, G.; Ryckaert, J. *Comput. Phys. Rep.* **1986**, *4*, 345.
(46) Allen, M.; Tildesley, D. *Computer Simulation of Liquids*; Clarendon Press: Oxford, 1989.
(47) Wang, J.; Boyd, R. J.; Laaksonen, A. *J. Chem. Phys.* **1996**, *104*, 7261.
(48) Skinner, J. L.; Park, K. *J. Phys. Chem. B* **2001**, *105*, 6716.
(49) Terashima, T.; Shiga, M.; Okazaki, S. *J. Phys. Chem.* **2001**, *114*, 5663.
(50) Gale, G. M.; Gallot, G.; Lascoux, N. *Chem. Phys. Lett.* **1999**, *311*, 123.
(51) Lawrence, C. P.; Skinner, J. L. *J. Chem. Phys.* **2003**, *119*, 3840.
(52) Chelli, R.; Ciabatti, S.; Cardini, G.; Righini, R.; Procacc, P. *J. Chem. Phys.* **1999**, *111*, 4218.
(53) Press, W. H.; Teukolsky, S. A.; Vetterling, W. T.; Flannery, B. P. *Numerical Recipes in Fortran, 2nd ed.*; Cambridge University Press: Cambridge, 1992.
(54) Harris, F. J. *Proc. IEEE* **1978**, *66*, 51.
(55) Edwards, D. M. F.; Madden, P. A. *Mol. Phys.* **1984**, *55*, 1163.
(56) Skaf, M. S.; Fonseca, T.; Ladanyi, B. M. *J. Chem. Phys.* **1993**, *98*, 8929.
(57) Handgraff, J.; van Erp, T. S.; Meijer, E. J. *Chem. Phys. Lett.* **2003**, *367*, 617.
(58) Pagliai, M.; Cardini, G.; Righini, R.; Schettino, V. *J. Chem. Phys.* **2003**, *119*, 6655.
(59) Yamaguchi, T.; Hidaka, K.; Soper, A. K. *Mol. Phys.* **1999**, *96*, 1159.
(60) Yamaguchi, T.; Hidaka, K.; Soper, A. K. *Mol. Phys.* **1999**, *97*, 603.